Check for updates

Received: 24 January 2021 | Revised: 30 April 2021 | Accepted: 2 May 2021

DOI: 10.1111/jace.17915

Journal of the American Ceramic Society

RESEARCH ARTICLE

Activation energies for crystallization of manganese-doped (K,Na)NbO_3 thin films deposited from a chemical solution

Leonard Jacques | **Veronika Kovacova** | **Jung In Yang** | **Susan Trolier-McKinstry**

Materials Science and Engineering Department and Materials Research Institute, The Pennsylvania State University, State College, Pennsylvania, USA

Correspondence
Leonard Jacques, Materials Science and Engineering Department and Materials Research Institute, The Pennsylvania State University, State College, Pennsylvania, USA.
Email: lcj6@psu.edu

Funding information
Center for Nanoscale Science and Technology, National Science Foundation, Grant/Award Number: DMR-1420620 and DMR-2011839

Abstract

Potassium sodium niobate (KNN) thin films are potentially useful for energy harvesting devices and for lead-free piezoelectric microelectromechanical systems. This work reports the activation energies for nucleation, growth and perovskite phase transformation from a 0.5% manganese-doped KNN 2-methoxyethanol-based solution modified with acetylacetone and excess alkali precursors. The films were annealed in a rapid thermal processor (RTP) with a hold step at temperatures from 500 to 550°C. The activation energies for perovskite transformation and growth, determined by electron micrograph observation, were 687 ± 13 and 194 ± 10 kJ/mol. The activation energy for nucleation was 341 ± 20 kJ/mol. Based on these data, crystallization in KNN is found to be nucleation-limited; thus, it should be possible to reduce the crystallization temperature by utilizing a seed layer which provides nucleation sites, provided the organics are removed from the film.

KEYWORDS

films, growth, KNN, nucleation

1 | INTRODUCTION

Piezoelectric potassium sodium niobate films are potential alternatives to lead zirconate titanate films for use in energy harvesting devices. These films are lead-free; their use would allay environmental concerns.[1,2] However, growing potassium sodium niobate (KNN) with high breakdown strength for such applications has proven a challenge, as reported in the literature.[3,4] Common processing problems include abnormal grain growth,[5] composition segregation,[3,6,7] formation of the undesired hygroscopic $K_4Nb_6O_{17}$ phase,[8,9] and difficulties managing excess alkali additions to the chemical solution.[3,4] In addition, little is known about the crystallization kinetics of KNN thin films.

Crystallization kinetics have been described for sputtered lead zirconate titanate (PZT) films by Kwok and Desu.[10] They reported the transformation of crystalline rosettes of PZT perovskite grains from a pyrochlore matrix. The activation energies for nucleation, growth, and perovskite transformation were determined from electron microscopy images using the Johnson-Mehl-Avrami-Kolmogorov (JMAK) kinetics approach.[11-15]

JMAK kinetics applies to polyhedral growth where growth is uniform in all directions in bulk samples,[11-13] and radial in thin films. This approach describes a locally random distribution with fine grains and the growth of circular rosettes at the onset of the phase transformation.[13] Nucleation events occur, activating rosette growth. Grains that nucleate at the same time have approximately the same size relative to each other throughout their growth.[11] Crystallization proceeds via multiple nucleation events, followed by growth.[13] It is presumed that the growth rate does not decrease with time; nuclei activated in a later nucleation event, or at a later time, will not grow larger than, or overtake nuclei activated earlier.[12] Thus, after the onset of crystallization, there should be observable sets of crystallized rosettes or grains on the film surface where each set consists of a unimodal distribution of rosette sizes. This is described in detail elsewhere.[11]

 © 2021 The American Ceramic Society

The nucleation and growth behavior associated with the perovskite phase transformation has been reported for PZT films as shown in Table 1.[10,16,17,18] There is variability in the reported results, with one chemical solution deposition study reporting the highest perovskite transformation energy of 610 kJ/mol, in contrast to data for sputtered PZT films, for which the transformation energy is reported to be 494 kJ/mol. CSD KNN solutions are known to require lengthier anneals than PZT, so a larger activation energy is possible.[8,9]

It was reported that the formation enthalpies for potassium niobate and sodium niobate, respectively, are −207 and −142 kJ/mol.[20] However, no in-depth study on the activation energies for nucleation and growth has been reported for KNN thin films grown using chemical solution deposition. Thus, this work studies activation energies for perovskite transformation, nucleation, and growth from a manganese doped KNN solution modified with acetylacetone as a chelating agent. Films were annealed at temperatures between 460 and 580°C; the best window of observation to determine an activation energy was between 500 and 550°C for annealing times between 5 and 100 s. A rapid thermal annealer was used in this work to provide fast ramp rates; this has been reported to encourage densification over nucleation in CSD films.[24] In other work, similar solutions were crystallized using a ramp rate of 10°C/s to process fully crystalline films, as reported elsewhere.[21] KNN films resulting from the solution synthesis and deposition process studied in this paper show promising overall electrical properties and moderate (100) crystallographic orientation at 1 μm thickness.[21,22] In addition, piezoelectric films have been derived from KNN solutions with added stabilizing agents such as polyvinylpyrrolidone.[23,24] Piezoelectric KNN films with strong (100) orientation,[25] and low leakage current properties by strontium doping[26] have also been derived from chemical solutions. Won et al. have also produced chemical solution derived manganese-doped KNN thin films with strong piezoelectric properties.[2]

2 | EXPERIMENTAL PROCEDURE

Solutions were prepared with 2-methoxyethanol solvent by weighing anhydrous sodium acetate (CH_3COONa) from Sigma–Aldrich 99% purity, anhydrous potassium acetate (CH_3COOK) from Sigma–Aldrich 99% purity, and manganese acetate tetrahydrate ($[CH_3COO]_2Mn\bullet 4H_2O$) from Sigma–Aldrich 99.95% purity, in plastic weigh boats and adding them to acetic anhydride.[21] In a separate flask, niobium ethoxide 99.95% purity $(CH_3CH_2O)_5Nb$ from STREM Chemicals was added to 2-methoxyethanol and weighed to achieve a final concentration of 0.4 M.[21] 10 mol% excess potassium acetate and 5 mol% excess sodium acetate were added to the precursor solution to account for losses due to volatility during processing.[3,4,27]

The acetate precursor complex in acetic anhydride was mixed in a 250 mL round bottom flask attached to a LABCONCO rotary evaporator. Upon mixing, the flask was placed in a silicone oil bath heated above 120°C. After mixing the solutions separately for 10 min, the acetate solution complex was vacuum-stripped to powder, removing the water.[28] The niobium complex in 2-MOE was mixed simultaneously in a dry box in an Erlenmeyer flask at room temperature for approximately 30 min before adding it to the alkali powders. The powders dissolved quickly upon addition of the niobium solution, and were refluxed in a rotary evaporator under 2 SCFH (standard cubic feet per hour) flow of argon at 106°C for 4 h. The resulting solution was amber colored; it was stored for at least one week in a refrigerator before spin-coating.

Prior to spin-coating, substrates were prepared by cleaving Pt(150 nm)/Ti(20 nm)/SiO_2(1 μm)/Si(0.5 mm) wafers from NOVA Electronic Materials into approximately 1 × 1 cm pieces. The chips were ultrasonically cleaned in isopropanol to remove dust particles.

Ten-milliliter plastic BD syringes and 0.1 μm filters with a PTFE (polytetrafluoroethylene) membrane and polypropylene

TABLE 1 A comparison between activation energies for different compositions of PZT synthesized and characterized by different methods along with data for $KNbO_3$

Material	Synthesis method	Measurement type	Activation energy (transformation, nucleation, growth) (kJ/mol)
PZT 53/47[10]	Sputtering, thin film	Scanning electron microscopy	494, 441, 112
PZT 60/40[17]	CSD, spin-coat	Optical	n/a, 286, 83 ± 6
PZT 80/20[17]	CSD, spin-coat	Optical	n/a, 296, 76 ± 5
PMN-PT (43% PT)[18]	Sol-gel, w/o PVP mod.	X-ray diffraction	305, n/a, n/a
PMN-PT (43% PT)[16]	Sol-gel, w/PVP mod.	X-ray diffraction	168, n/a, n/a
PZT 40/60[16]	Sol-gel, 100°C/s ramp	X-ray diffraction	610, n/a, n/a
$KNbO_3$[19]			216, n/a, n/a

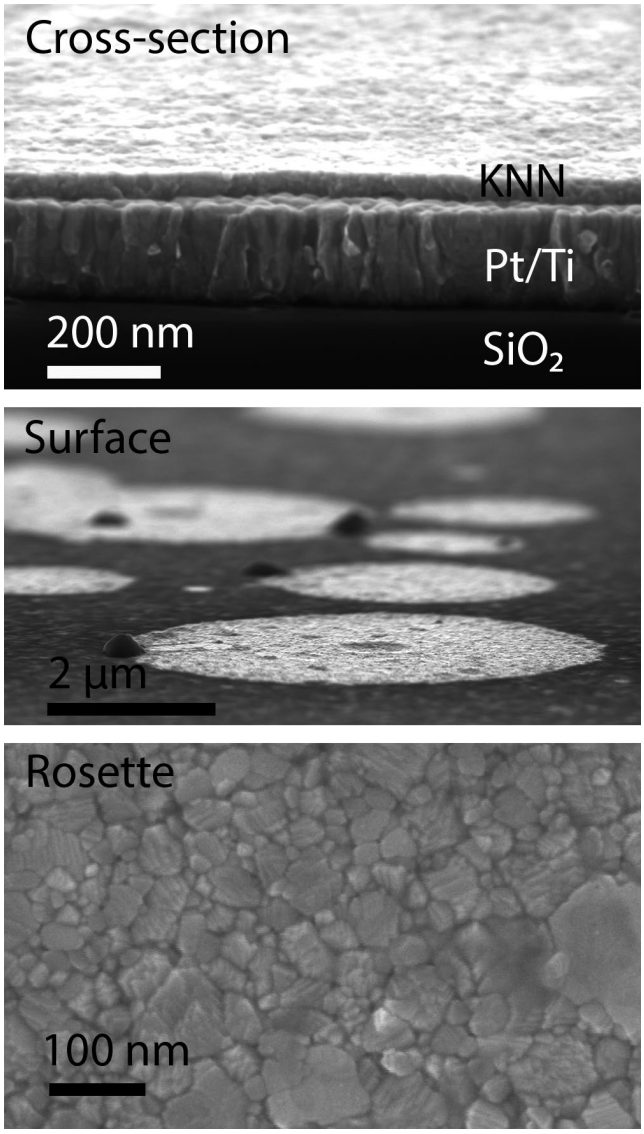

FIGURE 1 Potassium sodium niobate (KNN) crystallizes as circular rosettes at the onset of growth. The thickness of the perovskite KNN layer is approximately 40 nm measured by the field emission scanning electron microscope (FESEM) cross-section images. The bottom image shows the crystallites within the rosette from the top surface

housing were used to deposit the solution onto wafers for spin coating. The substrate was coated dynamically at a speed of 600 RPM and ramped to 3000 RPM for 30 s immediately after dispensing to form an even layer. This process was followed by heat treatment on hotplates with steel surfaces. The deposited film was dried at 200°C for 2 min, followed by pyrolysis at 300°C for 3 min, and a second pyrolysis step at 430°C for 3 min.[21,29] Acetylacetone functions as a chelating agent and makes the solution more stable against attack by water.[30] Consequently, acetylacetone ligands are difficult to pyrolyze and result in organics retained to temperatures near the crystallization temperature.[21,28] Retained organics hinder nucleation in chemical deposition processes[28]; therefore, the

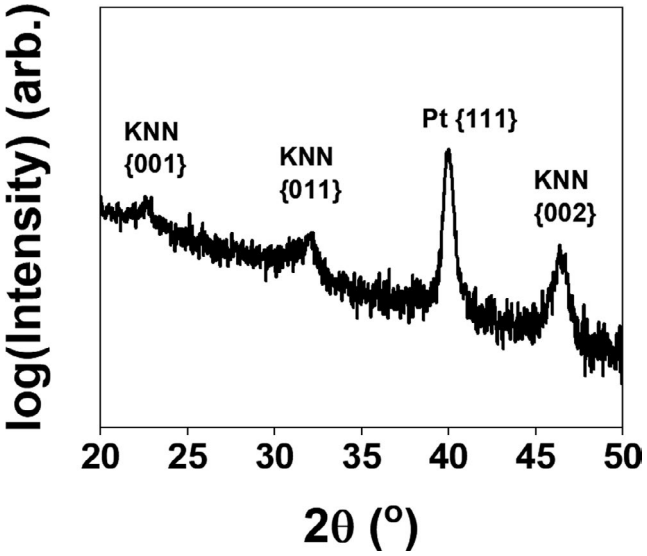

FIGURE 2 Glancing incidence X-ray diffraction was performed on a partially crystalline potassium sodium niobate (KNN) film that was annealed at 525°C for 40 s. Pseudocubic indices are used

activation energies reported here may differ from those of an unmodified solution.

Pyrolysis was immediately followed by a rapid thermal anneal at 500, 525, or 550°C at a ramp rate of approximately 90°C/s for annealing times between 5 and 100 s. All samples were deposited within 105 min to minimize potential solution aging effects.[21,28] Deposited layers were approximately 40 nm thick (see Figure 1).

A field emission scanning electron microscope (FESEM) (Zeiss Merlin) was used to obtain high resolution images of the KNN surface and cross-sections at a 5 kV accelerating voltage. Direct observation of FESEM images was used to determine the activation energies for perovskite transformation, growth, and nucleation.[10] The MATLAB® Image Segmenter application was used to determine the volume fraction of the crystallized perovskite phase over 8 to 10 images of the surface of each sample. The rosette sizes generated from the first nucleation event were averaged using the ImageJ application[31]; 10 to 30 rosettes on each sample were studied.[11] Additionally, the number of observable rosettes was counted manually over 8 to 10 images of each sample. The perovskite phase was confirmed by Glancing Incidence X-ray Diffraction (GIXRD) with an incidence angle of 1°, and Fourier Transform Infrared Spectroscopy (FTIR).

3 | RESULTS AND DISCUSSION

Annealed partially crystalline KNN films produced circular rosettes spanning the whole thickness of the film (see Figures 1–3). Perovskite KNN crystallites were on the order of 15 nm upon formation at the rosette perimeters. Grains

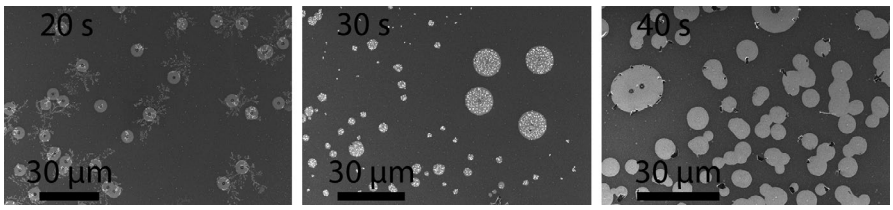

FIGURE 3 The progression of crystallization of potassium sodium niobate (KNN) to the perovskite phase from the amorphous phase at 525°C and 20, 30, and 40 s. Note changes in the size of the scale bar

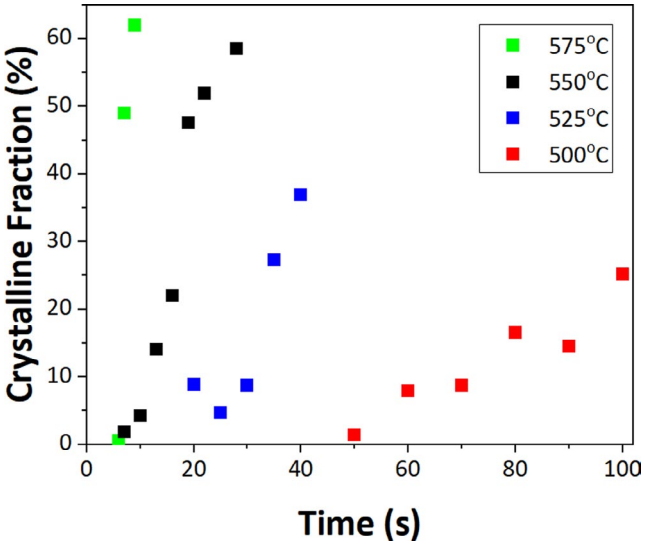

FIGURE 4 The progression of crystallization at temperatures from 500 to 575°C. Crystallization was too rapid at 575°C to observe for this method

at the center of rosettes grew to over 100 nm in dimension. Glancing incidence X-ray diffraction confirmed the presence of the perovskite phase (see Figure 2). In addition, FTIR confirmed an increasing intensity of the Nb-O vibration absorption with increasing volume fraction crystallized. Crystallization was not observed for heat treatment temperatures under 500°C and was too fast to quantify above 550°C (see Figure 4).

The activation energy for growth, the difference between adsorption and desorption energies for adatoms,[32] was calculated from early stages of rosette growth before extensive soft impingement and coalescence. Soft impingement reduces the concentration of reactants in the vicinity of a rosette and can hinder nucleation due to a local depletion region.[10] Rosettes grow radially outward as a disk, where the growth rate is proportional to the number of sites on the rosette perimeter.[11] Calculations of the activation energy involved data from 500, 525, and 550°C. Each of the data sets captured the first nucleation event. After a nucleus is activated, it goes through a phase of slow growth, followed by a constant growth rate[13]; this is consistent with the description of growth provided by Johnson and Mehl.[14] A constant growth rate was observed for KNN, as shown in Figure 5A. The incubation period where growth is slow was ignored when observing the growth rate.

The radii (r_{max}) of the rosettes were used to determine the rate constant, k.[10]

$$r_{max} = kt^n \tag{1}$$

$$\ln r_{max} = \ln k + n \ln t \tag{2}$$

The y intercept of the plot in Figure 5A is the natural log of the rate constant, ln(k). The time exponent n indicates the type of crystal growth. The n values were 1.40 ± 0.11, 1.32 ± 0.08, and 1.10 ± 0.08 for 550, 525, and 500°C, respectively. By comparison, exponents near 1 were observed in Kwok and Desu's work on sputtered PZT[10] where no excess secondary phases were observed on the surface of the film. An exponent of 1 indicates surface-mediated growth from the perimeter of the rosettes in thin films with two-dimensional growth,[10] where adatoms transfer across the circumference (interface).[11] The n values greater than 1 observed in this work indicate either an increase in the dimensionality of growth or rapid growth.[29] As will be reported in detail elsewhere, a higher concentration of potassium was observed at rosette perimeters on EDS spatial composition maps. In addition, the presence of dendrites on the film surface in Figure 3, indicates rapid crystal growth, which would be consistent with $n > 1$.[33]

The rate constant, k, was used to calculate the activation energy (E_a) for growth[10]:

$$\ln k = \ln A + \left(\frac{-E_a}{R}\right)\left(\frac{1}{T}\right) \tag{3}$$

where R is the universal gas constant and T is the absolute temperature. The goodness of fit exceeded 0.98 on all regression lines for growth, as shown in Figure 5A. The activation energy for perovskite growth was calculated to 194 ± 10 kJ/mol. The error was determined from the linear regression on the Arrhenius plot, as seen in Figure 5B.

In materials systems such as KNN with volatile sodium and potassium constituents, changes in concentration can change the time scale of the crystallization reaction. However, the high goodness of fit on the Arrhenius plots (see Figure

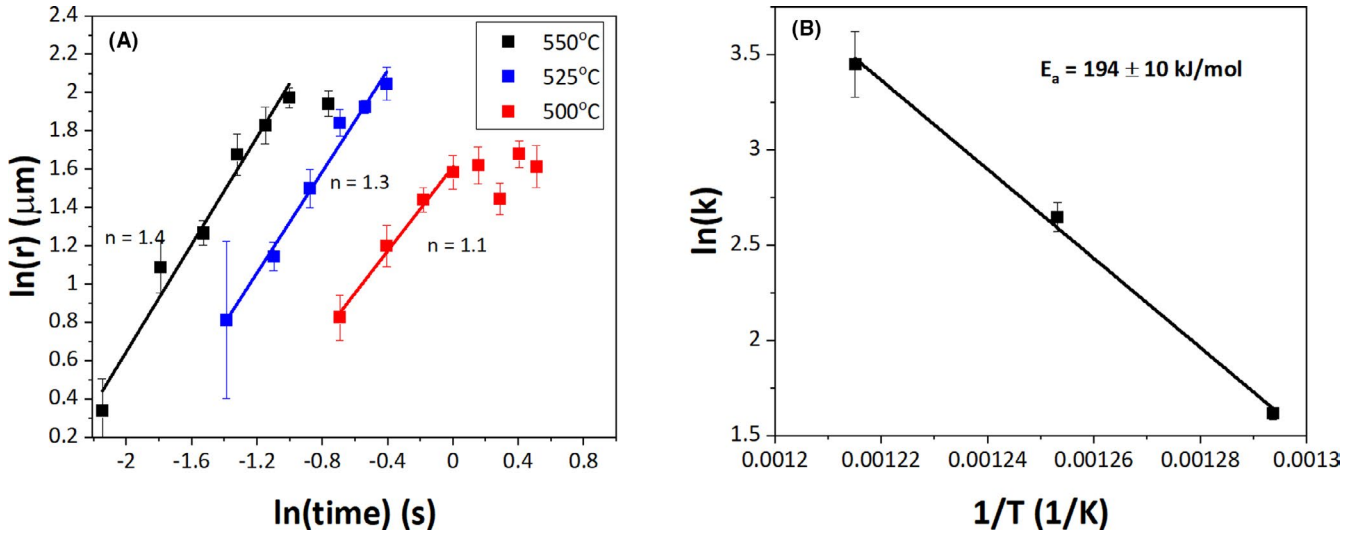

FIGURE 5 (A) Plot of radius, *r*, of the rosettes as a function of time. (B) The activation energy for growth was calculated from the temperature (*T*) dependence of the rate constant (*k*). The rate constants at 500, 525, and 550°C have an Arrhenius relationship from which the activation energy for growth was determined. The large error bar for some of the data at 525°C was associated with some dendritic growth in those samples

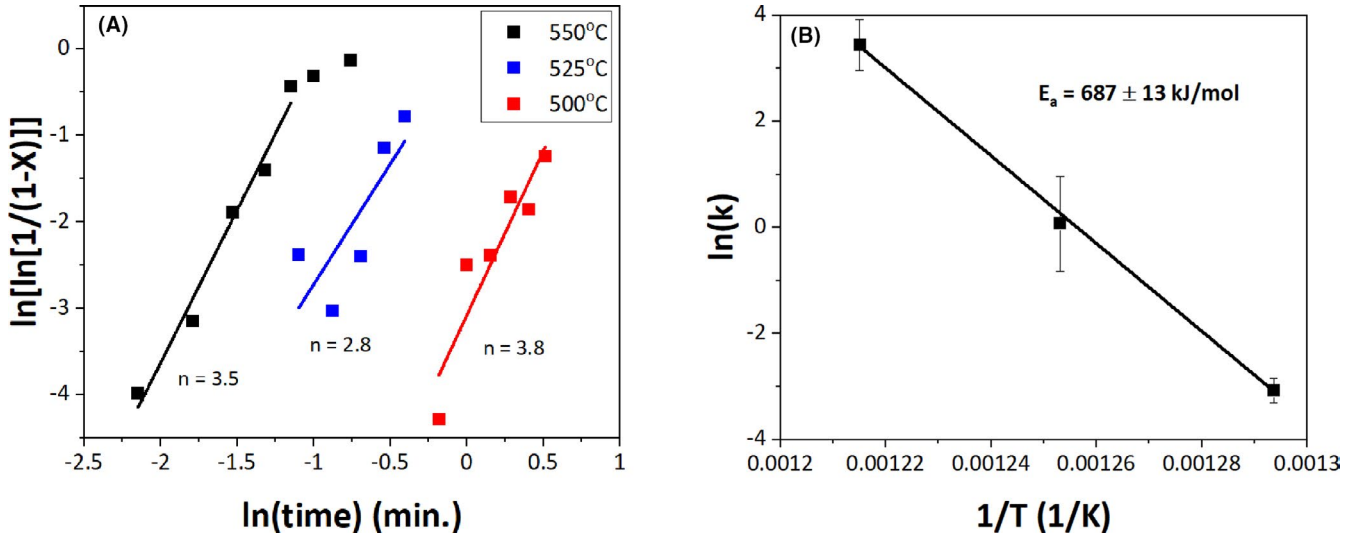

FIGURE 6 (A) The *y* intercepts of the Avrami–Erofeev graph are the rate constants, ln(*k*). (B) The Arrhenius relationship from which the activation energy for perovskite phase transformation was extracted

5B) suggest the time scale of crystallization for the samples was consistent for all the data sets.

The perovskite transformation energy was calculated by measuring the volume fraction crystallized (see Figure 4). Rosettes were assumed to be perfect cylinders through the thickness of the film, so only the surface area of the rosettes were measured using FESEM images. Over multiple trials, growth nearly stopped around 60 vol% crystallized for 525 and 550°C. Similarly over multiple trials for a crystallization temperature of 500°C, no clear saturation was observed, neither was a transformation over 30% observed.

It remains unclear why crystallization saturated at a lower fraction at 500°C. One hypothesis is that either depletion of volatile sodium or accumulation of residual potassium around the rosette perimeter increased the time scale, τ, of the crystallization reaction[10] at longer anneal times, so the kinetics were delayed. Therefore, only short anneal times, which scale approximately linearly on the Avrami–Erofeev plot in Figure 6A, were used in this study. At temperatures below 500°C crystallization was not observed.

Crystallization saturation may be due to a number of potential factors, including intermediate carboxylate phases which are difficult to decompose[28] or progressive

composition segregation of excess alkali at the perimeter of the rosettes, for example. The observed deviations from the fitted JMAK curves may be due to randomness of the nucleation rate coupled with changes in the solution as it ages in the syringe throughout a deposition process.[28] A small change in the volume free energy, due to a change in viscosity, for example, can have a profound effect on nucleation density. A 10% decrease in the change in volume free energy upon crystallization can result in an order of magnitude decrease in nucleation density.[28] Future work is in progress to reveal the processing details in CSD KNN films which are responsible for the observed deviations.

The perovskite transformation energy was calculated using the Avrami–Erofeev kinetic equation.[10,14]

$$X_t = 1 - \exp\,(-kt^n) \tag{4}$$

$$\ln\left(\ln\frac{1}{1-X_t}\right) = \ln k + n\ln t \tag{5}$$

where X_t is the volume fraction of the film converted to the perovskite phase. The rate law exponents, n, were 3.8 ± 0.8, 2.8 ± 1.2, and 3.5 ± 0.3 for 550, 525, and 500°C, respectively. The maximum theoretical rate law is 3 for phase transformation in a thin film. As discussed earlier, higher-than-normal rate laws could indicate rapid crystallization due to excess alkali concentrations on the film surface.[11] While an apparently lower rate law exponent of 2.8 ± 1.2 was observed for the data at 525°C, the larger error bars preclude any conclusion that there is a statistically significant difference between the exponents.

The deviations from linearity in the $\ln(\ln(\frac{1}{1-x}))$ versus ln(-time) plot for 500°C, shown in Figures 4 and 6A, are probably due to randomness in the nucleation rate. The last two points taken from the temperature 550°C data set were not included for calculation of the activation energy due to the characteristic "fall off" of experimental points as the JMAK curve begins to flatten.[11]

The total activation energy for perovskite transformation was calculated to 687 ± 13 kJ/mol. The large activation energy for perovskite transformation compared to relatively small activation energies measured for growth emphasize the crystallization kinetics of KNN thin films from this CSD route are nucleation dominated. Accurate observation of the volume fraction crystallized is required to determine the activation energy of perovskite transformation. This could not be performed with conventional measures such as XRD and FTIR due to preferred orientation and inability to confirm that peaks corresponding Nb-O are the perovskite phase, respectively. Instead, comparison to a theoretical model was used to test the validity of these results, as shown later.

Two activation energies for nucleation from the average nucleation rate and the maximum apparent nucleation rate were calculated. Variances in the nucleation density between samples resulted in difficulties in calculating the activation energy for nucleation via the direct observation approach with FESEM images. At 500, 525, and 550°C the nucleation rates were calculated from the four shortest viable anneal times. At longer anneal times, coalescence of the rosettes made it difficult to count the number of active or growing nuclei. JMAK kinetics describes a constant nucleation rate where all "phantom" nuclei must be counted as well.[11,13] "Phantom" nuclei are nuclei which are unobservable because they have been overtaken by a growing nucleus. Since the apparent nucleation rate was not constant in this study, it was difficult to determine an activation energy for nucleation by direct observation and counting the nucleation densities.

The nucleation rate was estimated per each sample by dividing the nucleation density by the time elapsed since nucleation began.[10]

$$\dot{N} = \frac{N_i}{\Delta t} \tag{6}$$

$$\ln \dot{N} = \ln A + \left(\frac{-E_a}{R}\right)\left(\frac{1}{\mathrm{T}}\right) \tag{7}$$

where N_i is the nucleation density at the later time step and Δt is the time elapsed since the onset of nucleation. The average nucleation rate ($\dot{N}$) in Figure 7A was calculated by averaging the individual nucleation rates at a given temperature.

Variations in nucleation density are due to the randomness of nucleation. The fluctuations in nucleation rate are reflected in the total perovskite transformation (see Figure 4), which illustrates that nucleation dominated the crystallization kinetics. For example, a high nucleation rate is observed at the onset of crystallization at 525°C, which is the cause of the fluctuation in volume percent crystallized in Figure 6A. A falling nucleation rate over time was reported by Kwok and Desu due to the decreasing concentration of reactants in the amorphous phase, and "soft impingement".[10] However, in this work a regime of falling nucleation rates was not observable. Therefore, the calculations for the activation energy for nucleation by direct observation are an approximation.

According to Johnson and Mehl, the nucleation density should always increase with time, however the growth of activated nuclei overtakes germs and smaller nuclei within the crystallized volume.[12,13] This reduces the number of observable nuclei as annealing time progresses, producing the "apparent" nucleation rate. As described elsewhere,[11] multiple "layers" of nucleation events coexist on the film along a time coordinate, but the first "layers" partially cover subsequent "layers" so they are unobservable. Therefore, calculating the activation energy from the nucleation rate requires information from all the "layers." For this measurement technique,

"phantom" nuclei are not counted, but they are accounted for in the total perovskite transformation energy[13] mentioned earlier.

FESEM backscatter images suggest the existence of phantom grains in KNN, since the KNN film appears thinner at the center of the rosettes where the germs were located (see Figure 8). Phantom grains appear as lighter-colored spots on backscatter electron images where more electrons scatter from the platinum substrate which has a higher atomic mass than the elements in KNN. A germ nucleus which has become active does not grow appreciably until the completion of its incubation period.[11,13] During this time, the active germ nuclei can be overtaken by a growing rosette and become undetectable on secondary electron images which were used for all image processing. The contrast on electron backscatter images due to the higher atomic number of Pt from the substrate indicate locations where germs which have become active, and were overtaken in their incubation period. Abrupt perturbations in the thickness of the KNN layer are otherwise not expected. This phenomenon is responsible for the inability to discern an accurate nucleation density by direct observation at longer anneal times.[10,11] Moreover, soft impingement and a high volume fraction transformed also introduced error in measurements of nucleation densities at long anneal times. For example, it is nearly impossible to determine a nucleation density via direct observation when nearly 50 vol% of the film had crystallized.

Due to the hinderances to determining the actual nucleation rate, two activation energy approximations for nucleation are provided, using the maximum apparent nucleation rate, and the average apparent nucleation rate at each temperature. The goodness of fit was greater than 0.99 on the Arrhenius plots for both methods. The activation energy for nucleation using the maximum nucleation rate is 341 ± 20 kJ/mol. The activation energy for nucleation using the average nucleation rate is 323 ± 5 kJ/mol. Higher activation energies for nucleation than growth confirm the transformation activation energy is dominated by nucleation.

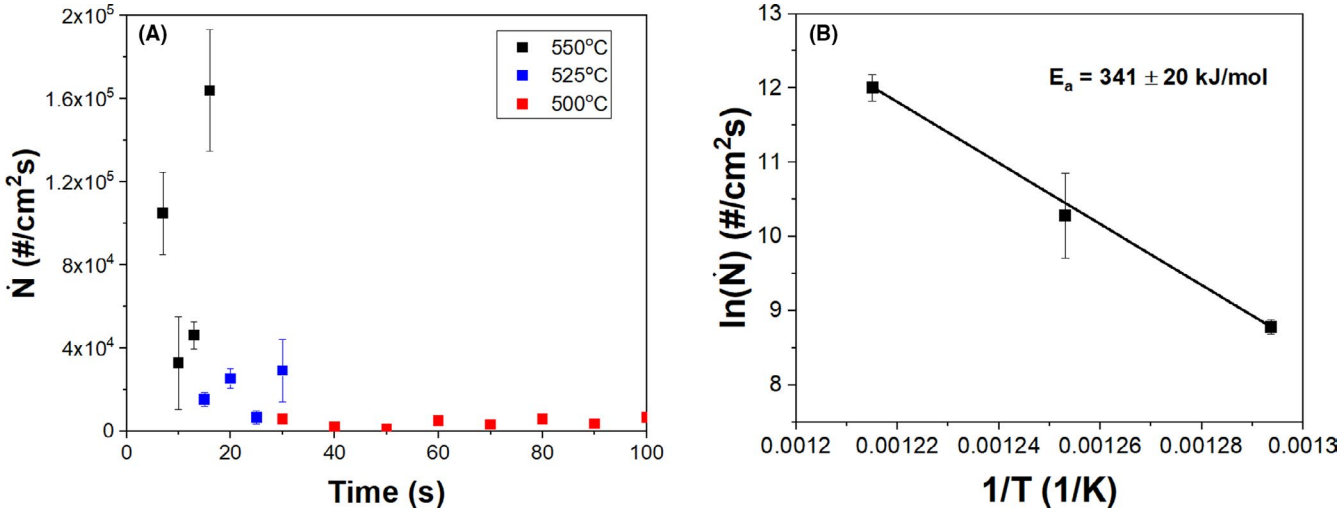

FIGURE 7 (A) The nucleation rate at the onset of crystallization as a function of the time for different crystallization temperatures. Both the average and maximum nucleation rates at the three temperature have an Arrhenius relationship. The activation energy for the maximum nucleation rate is plotted in (B)

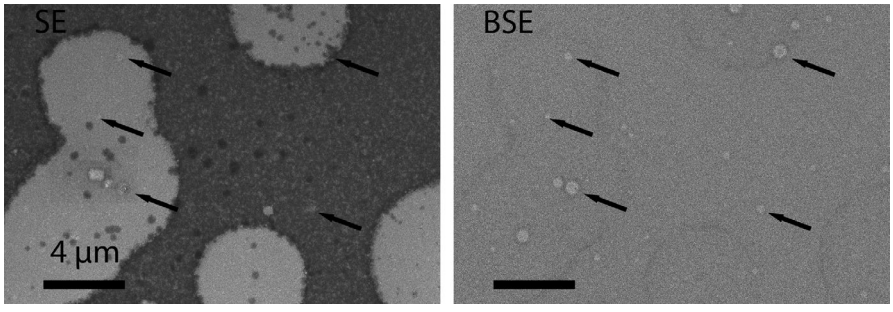

FIGURE 8 Field emission scanning electron microscope (FESEM) secondary electron image (left) and back-scatter electron (BSE) image (right) of the same section of film. Phantom grains which are not observable on the secondary electron image are observable on the BSE image as lighter colored dots, some of which are indicated by arrows. Nuclei in the amorphous section are hindered from growing due to "soft impingement"[10]—the depletion in the concentration of reactants near crystallized rosettes

A theoretical model for nucleation and growth contributions to the transformation energy was applied to the experimental results to check the validity of the calculated values for the activation energies.[34]

$$\Delta H = E_{A,n} + (m-1)\,E_{A,g} \quad (8)$$

where ΔH is the perovskite transformation energy. $E_{A,n}$ is the activation energy for nucleation and $E_{A,g}$ is the activation energy for growth. The coefficient m depends on the dimensionality, where $m = 3$ for two-dimensional growth modeled here. Therefore,[33]

$$\Delta H = E_{A,n} + 2E_{A,g} \quad (9)$$

Using the numbers calculated in this study and the maximum nucleation rate:

$$\Delta H = 341\ \text{kJ/mol} + 2\,(194\ \text{kJ/mol}) = 729\ \text{kJ/mol} \quad (10)$$

Using the numbers calculated in this study and the average nucleation rate:

$$\Delta H = 323\ \text{kJ/mol} + 2\,(194\ \text{kJ/mol}) = 711\ \text{kJ/mol} \quad (11)$$

The theoretical prediction of the perovskite transformation energy falls within error bounds for the experimental perovskite transformation energy of 687 ± 13 kJ/mol, if the tolerances for error are considered. Likewise, the two different values for $E_{A,n}$ fall within error bounds of each other.

It is clear that in KNN films, as in PZT, the activation energy for nucleation exceeds that of growth substantially. This suggests that nucleation will be the rate-limiting process. It also suggests that if the nucleation can be adequately controlled, it should be possible to use nucleation from the substrate only to control film orientation.

Since organics remain in the film at the onset of nucleation, it is hypothesized that the activation energy for nucleation may change for a solution prepared with a different synthesis method. Factors that can influence the crystallization behavior include the solution chemistry, solution age, substrate, doping, crystallization environment, and alkali volatility. Therefore, the results of this study are pertinent to films deposited from the solution method described here. Since remaining organics may still exist in the film at the moment of crystallization, this activation energy may also account for the energy required to decompose carboxylate species from the thin film prior to crystallization.[11] It is also possible that remaining organics act as nucleation sites and bias the activation energy for nucleation. In this case, growing KNN via other methods may have different values for the activation energies. A subsequent paper will report on the decomposition processes and composition fluctuations observed during heat treatment for chemical solution deposited (CSD) KNN films from these different solution synthesis methods.

TABLE 2 A summary of the activation energies for the method described in this paper

Category	Activation Energy kJ/mol
Total perovskite transformation	687 ± 13
Growth	194 ± 10
Nucleation (direct observation)	341 ± 20

4 | CONCLUSIONS

In conclusion, the JMAK kinetic approach was used to determine the total perovskite transformation energy, the nucleation energy, and the growth activation energy for the amorphous to perovskite transition of KNN films prepared by a chemical solution deposition method using acetic anhydride and 2-methoxyethanol as the solvents. The activation energies are presented in Table 2. Experimental results agree with theoretical predictions on the link between these three activation energies as described by Ranganathan and Heimendahl.[34] Crystallization of KNN is found to be nucleation-limited, such that crystallization orientation can be achieved by using a seed layer.

ACKNOWLEDGEMENTS

This project is a portion of the Center for Nanoscale Science, a Materials Research Science and Engineering Center (MRSEC) supported by the National Science Foundation under grant DMR-2011839 (2020–2026) and DMR-1420620. The authors give special thanks to Bangzhi Liu, Tawanda Zimundi, and Joshua Stapleton of the Penn State MRI for and taking FESEM-EDS images and performing FTIR to help with composition and phase identification.

ORCID

Leonard Jacques https://orcid.org/0000-0001-5032-0019
Veronika Kovacova https://orcid.org/0000-0002-9281-3732
Susan Trolier-McKinstry https://orcid.org/0000-0002-7267-9281

REFERENCES

1. Saito Y, Takao H. High performance lead-free piezoelectric ceramics in the (K, Na)NbO_3-$LiTaO_3$ solid solution system. Ferroelectrics. 2006;338(1):17–32.
2. Won SS, Lee J, Venugopal V, Kim DJ, Lee J, Kim IW, et al. Lead-free Mn-doped ($K_{0.5}$,$Na_{0.5}$)NbO_3 piezoelectric thin films for MEMS-based vibrational energy harvester applications. Appl Phys Lett. 2016;108(23):232908.

3. Kupec A, Uršič H, Frunză RC, Tchernychova E, Malič B. Microstructure-dependent leakage-current properties of solution-derived $(K_{0.5}Na_{0.5})NbO_3$ thin films. J Eur Ceram Soc. 2015;35(13):3507–11.
4. Ahn CW, Lee SY, Lee HJ, Ullah A, Bae JS, Jeong ED, et al. The effect of K and Na excess on the ferroelectric and piezoelectric properties of $K_{0.5}Na_{0.5}NbO_3$ thin films. J Phys D J Phys D Appl Phys. 2009;42(21):215304.
5. Pop-Ghe P, Stock N, Quandt E. Suppression of abnormal grain growth in $K_{0.5}Na_{0.5}NbO_3$: Phase transitions and compatibility. Sci Rep. 2019;9(1):1–10.
6. Kupec A, Malic B, Tellier J, Tchernychova E, Glinsek S, Kosec M. Lead-free ferroelectric potassium sodium niobate thin films from solution: Composition and structure. J Am Ceram Soc. 2012;95(2):515–23.
7. Malic B, Jenko D, Holc J, Hrovat M, Kosec M. Synthesis of sodium potassium niobate: A diffusion couples study. J Am Ceram Soc. 2008;91(6):1916–22.
8. Kimura H, Tanahashi R, Zhao H, Yao Q. Weak ferroelectricity of potassium niobate $K_4Nb_6O_{17}$ single crystal grown by pulling down technique. Mater Lett. 2012;1(84):16–9.
9. Zhong T, Tang J, Zhu M, Hou Y, Wang H, Yan H. Synthesis and characterization of layered niobate $K_4Nb_6O_{17}$ thin films by niobium-chelated precursor. J Cryst Growth. 2005;285(1–2):201–7.
10. Kwok CK, Desu SB. Formation kinetics of $PbZr_xTi_{1-x}O_3$ thin films. J Mater Res. 1994;9(7):1728–33.
11. Fanfoni M, Tomellini M. The Johnson-Mehl-Avrami-Kohlmgorov model: a brief review. Il Nuovo Cimento D. 1998;20(7–8):1171–82.
12. Avrami M. Kinetics of phase change. I general theory. J Chem Phys. 1939;7(12):1103–12.
13. Avrami M. Kinetics of phase change. II transformation-time relations for random distribution of nuclei. J Chem Phys. 1940;8(2):212–24.
14. Johnson WA, Mehl RF. Reaction kinetics in processes of nucleation and growth. Am Inst Min Eng. 1939:1–27.
15. Kolmogorov AN. On the statistical theory of the crystallization of metals. Bull Acad Sci USSR Math Ser. 1937;1(3):355–9.
16. Griswold EM, Weaver L, Sayer M, Calder ID. Phase transformations in rapid thermal processed lead zirconate titanate. J Mater Res. 1995;10(12):3149–59.
17. Peng CH, Desu SB. Investigation of structure development in MOD $Pb(Zr_xTi_{1-x})O_3$ films by an optical method. MRS Online Proceedings Library Archive. 1991;243.
18. Du ZH, Zhang TS, Zhu MM, Ma J. Perovskite crystallization kinetics and dielectric properties of the PMN-PT films prepared by polymer-modified sol-gel processing. J Mater Res. 2009;24(4):1576–84.
19. Ko JB, Hong JH. Structural and thermal properties of potassium niobate glasses for an application in electro-optical product design and manufacture. J Ceram Process Res. 2010;11(1):116–9.
20. Ozmen O, Ozsoy-Keskinbora C, Suvaci E. Chemical stability of $KNbO_3$, $NaNbO_3$, and $K_{0.5}Na_{0.5}NbO_3$ in aqueous medium. J Am Ceram Soc. 2018;101(3):1074–86.
21. Kovacova V, Yang JI, Jacques L, Ko SW, Zhu W, Trolier-McKinstry S. Comparative solution synthesis of Mn doped (Na, K)NbO_3 thin films. Chem A Eur J. 2020;26(42):9356–64.
22. Kovacova V, Yang JI, Jacques L, Yeo HG, Lanari V, Rahn C, et al. Comparison of $K_{0.5}Na_{0.5}NbO_3$ and $PbZr_{0.52}Ti_{0.48}O_3$ compliant-mechanism-design energy harvesters. J Appl Phys. 2021;129(11):114101.
23. Wang L, Yao K, Chin GP, Ren W. Volatilization of alkali ions and effects of molecular weight of polyvinylpyrrolidone introduced in solution-derived ferroelectric $K_{0.5}Na_{0.5}NbO_3$ films. J Mater Res. 2009;24(12):3516–22.
24. Wang Y, Yao K, Sharifzadeh Mirshekarloo M, Tay FEH. Effects and mechanism of combinational chemical agents on solution-derived $K_{0.5}Na_{0.5}NbO_3$ piezoelectric thin films. J Am Ceram Soc. 2016;99(5):1631–6.
25. Kwak J, Kingon AI, Kim SH. Lead-free ($Na_{0.5}$, $K_{0.5}$) NbO3 thin films for the implantable piezoelectric medical sensor applications. Mater Lett. 2012;82:130–2.
26. Vojisavljević K, Vrabelj T, Uršič H, Malič B. Effects of strontium doping on microstructure and functional properties of solution-derived potassium sodium niobate thin films. Process Appl Ceram. 2020;14(3):231–41.
27. Schneller T, Waser R, Kosec M, Payne D, editors. Chemical Solution Deposition of Functional Oxide Thin Films. Vienna: Springer Vienna; 2013.
28. Yanovskaya MI, Obvintseva IE, Solovyova LI, Kovsman EP, Vorotilov KA, Vasilyev VA. Alkoxy-derived ferroelectric PZT films: the effect of lead acetate dehydration techniques and lead content in the electrochemically prepared solutions on the properties of the films. Integrated Ferroelectrics. 1998;19(1–4):193–209.
29. Wiegand S, Flege S, Baake O, Ensinger W. Influence of different heat treatment programs on properties of sol–gel synthesized $(Na_{0.5}K_{0.5})NbO_3$ (KNN) thin films. Bull Mater Sci. 2012;35(5):745–50.
30. Röscher M, Schneller T, Waser R. Comments on the processing of the niobium component for chemical solution derived niobium oxide-based thin-films. J Sol-Gel Sci Technol. 2010;56(3):236–43.
31. Schneider CA, Rasband WS, Eliceiri KW. NIH image to imageJ: 25 years of image analysis. Nat Methods. 2012;9(7):671–5.
32. Holloway PH, Hudson JB. Kinetics of the reaction of oxygen with clean nickel single crystal surfaces: I. Ni (100) surface. Surf Sci. 1974;43(1):123–40.
33. Trivedi R, Kurz W. Dendritic growth. Int Mater Rev. 1994;39(2):49–74.
34. Ranganathan S, Von Heimendahl M. The three activation energies with isothermal transformations: applications to metallic glasses. J Mater Sci. 1981;16(9):2401–4.

How to cite this article: Jacques L, Kovacova V, Yang JI, Trolier-McKinstry S. Activation energies for crystallization of manganese-doped (K,Na)NbO_3 thin films deposited from a chemical solution. *J Am Ceram Soc*. 2021;00:1–9. https://doi.org/10.1111/jace.17915